Journal of Chromatography, 520 (1990) 271–285
Elsevier Science Publishers B.V., Amsterdam

CHROMSYMP. 1920

Non-equilibrium analytical focusing field-flow fractionation using intrinsic hydrodynamic force and integral Doppler anemometry

V. L. KONONENKO* and J. K. SHIMKUS
Institute of Chemical Physics, U.S.S.R. Academy of Sciences, Kosygin str. 4, 117334 Moscow (U.S.S.R.)

ABSTRACT

Experimental and theoretical results are presented on the analytical focusing field-flow fractionation (FFFF) of micrometre-sized particles, using the intrinsic hydrodynamic force for separation and integral Doppler anemometry (IDA) for detection of fractions. The intrinsic hydrodynamic force, new in FFF practice, which naturally arises in a shear flow, allows FFFF to be implemented without the application of any external force field to a channel. A stationary and uniform concentration distribution of particles in a flow is maintained at the channel entrance, and different fractions are detected under the essentially non-equilibrium conditions in the process of transformation of initially uniform concentration profiles into laterally inhomogeneous profiles in the course of the advancement of particles along the channel. The IDA detection of fractions is made not at the outlet, but at intermediate distances along the channel, as soon as the separation of fractions across the channel is started. The necessary theory of the transient concentration distributions of particles in a flow is considered in a non-diffusive approximation for arbitrary profiles of flow velocity and lateral force, and specified for the case of intrinsic hydrodynamic force.

INTRODUCTION

Recently a new technique for the rapid measurement of the transverse concentration profiles of particles in a flow was introduced, namely integral Doppler anemometry (IDA) [1–4]. When applied to analytical field-flow fractionation (FFF) problems [5–7], this technique allows the detection of fractions just inside the channel instead of at its outlet, as is usually done. This promises a considerable increase in analysis rate and a decrease in the necessary channel length in classical equilibrium FFF systems [5–17]. The point is that the detection of fractions can be started immediately after the establishment of transverse equilibrium of particles in a channel, and it is not necessary to wait until the much longer longitudinal separation of fractions is completed [1–4]. Moreover, the use of IDA opens up some new possibilities that are inaccessible with traditional recording techniques in FFF. They include the possibility of non-equilibrium analytical FFF when different particle species are detected not after [5–17] but during the process of their equilibration across the channel. This promises a further shortening of analysis times and the channel length in FFF. It has been shown [2–4] that the most advantageous for IDA applications are the focusing or hyperlayer FFF systems (FFFF) considered by Janča, Giddings and others

0021-9673/90/$03.50

[8–17]. In such systems, as they were theoretically suggested [8–14] and experimentally implemented [15–17], a steady-state transverse concentration distribution of particles in a channel flow is formed owing to the action of two lateral fields: a strong primary field (centrifugal, electrical or transverse fluid flow) and a counteracting secondary field (gradient of solvent density or pH). As a result, after the transverse equilibrium is set, the particles of different species are concentrated near the appropriate points of channel cross-section, where the corresponding net acting forces are zero [8–12]. For the negligibly small diffusion of particles the resulting concentration profiles would be the sum of delta-functions, but the diffusion process makes them the sum of Gaussian-type curves [9,11]. For these laterally equilibrium conditions the concentration profiles of fractions, retention ratios and effective plate heights have been considered theoretically [9–14].

The results of our previous experiments [4] and theoretical studies [2,3] demonstrated the possibility of implementing an FFFF system with IDA detection without the application of any external field to a channel. This possibility is based on the so-called tubular pinch or Segre–Silberberg effect [18,19], the essence of which is that the particle in a laminar channel flow undergoes the action of transverse focusing hydrodynamic forces due to some inertial effects in a fluid. The magnitude of this force depends on the flow velocity and the ratio of particle diameter to channel width, but the focusing positions are independent of the particle dimensions and lie symmetrically between the channel centre and its walls [4,18,19]. Thus, after establishment of transverse equilibrium, all the particle species would be focused together in the same lateral position. However, during the equilibration process they are separated laterally owing to the different lateral velocities gained under the action of the Segre–Silberberg hydrodynamic force. Hence, in such a non-equilibrium situation, the sum of the transient concentration profiles of a fraction can be registered using the IDA technique, as was done for a suspension flow of monodisperse particles [4]. Provided that these transient profiles have characteristic maxima, analogous to those recorded previously [4], this solves the task of analytical fractionation.

In this paper we present experimental evidence for analytical focusing field-flow fractionation of particles under non-equilibrium conditions, with no external field applied to the channel, using intrinsic hydrodynamic focusing force (Segre–Silberberg force) and IDA recording technique. The theoretical relationships necessary for the description of the transient concentration profiles of particles under these conditions, and for the shape of IDA spectra, are developed. The experimental set-up and conditions for implementation of this separation process and for recording by means of the IDA technique are described.

THEORETICAL

General relationships

The theory of focusing or hyperlayer FFF was developed in a series of papers [8–14], which considered the concentration distribution of particles over the channel after the establishment of particle equilibrium across the channel under the action of a lateral force. Under such laterally equilibrium conditions the transverse concentration profile of the particle system in a channel flow can be well approximated by the sum of Gaussian-type curves centred at the appropriate stationary focusing points

[9,11,14]. The intrinsic hydrodynamic focusing force, used in our previous [4] and present experiments, has two specific features. First, the particles driven by this force reach their lateral equilibrium positions in a flow very far from the channel entrance. Second, these equilibrium positions are identical for all the particles [18,19]. In contrast, for intermediate distances from the entrance, where the transverse equilibrium is not yet established, the lateral positions of concentration peaks and their specific shapes depend strongly on these distances, and also on the particle size and the specific profile of the acting force. This opens up the possibility of the analytical fractionation of particles, but means operating under non-equilibrium, although stationary, conditions. This necessitates the calculation of the essentially non-equilibrium lateral concentration profiles along the channel, corresponding to the specific profile of the intrinsic hydrodynamic force acting on the particles. The profile of this force has been calculated numerically for plane Poiseuille flow [19] and, as we have verified, can be well approximated by the following equation:

$$F_x = F_0\varphi(x); \qquad F_0 = \frac{9\pi}{4}v_{\parallel}^2\frac{\rho_0 a^2}{1-x_f^2}\left(\frac{a}{h}\right)^2;$$
$$\varphi(x) = x(x_f^2 - x^2); \qquad x_f \approx 0.62 \tag{1}$$

where $v_{\parallel}$ is the maximum flow velocity, ρ_0 is the fluid density, a is the particle radius, h is the flat channel half-width, $\varphi(x)$ is the dimensionless force profile and x_f is the focusing point (our previous [4] and also the present measurements show that the focusing point can be closer to the centre, but this makes no significant difference). We use the dimensionless coordinate system in the units of h with the z-axis along the flow, the x-axis perpendicular to the channel wall and the origin in the middle of a channel. Eqn. 1 shows that for $|x| > x_f$ the force is directed inside the channel [$\varphi(x) > 0$ for $-1 \leqslant x < -x_f$, $\varphi(x) < 0$ for $x_f < x \leqslant 1$], whereas for $|x| < x_f$ it is directed from the centre, tending to concentrate the particles near the two symmetrical planes $x = \pm x_f$. If the stationary transverse concentrational profile of particles $C_0(x_0)$ is maintained at the channel entrance, then the transient concentration distribution $C(x,z)$ can be found as a solution of the stationary equation of convective diffusion along the channel. We shall assume that the particles are sufficiently large to neglect their Brownian movement. In this case the particle velocity $\vec{v}$ is completely determined by the balance of the driving force and Stokes viscous force, and the convective diffusion equation reduces to the usual continuity equation:

$$\mathrm{div}[C(x,z)\vec{v}] = 0;$$
$$v_x = \frac{F_0}{6\pi\eta a}\varphi(x); \qquad v_y = 0; \qquad v_z = v_{\parallel}u(x); \tag{2}$$
$$\varphi(x)\frac{\partial C(x,z)}{\partial x} + \mu u(x)\frac{\partial C(x,z)}{\partial z} + C(x,z)\frac{\partial\varphi(x)}{\partial x} = 0;$$
$$\mu = \frac{6\pi\eta a v_{\parallel}}{F_0} \equiv \frac{v_{\parallel}}{v_{\perp}}$$

where η is the fluid viscosity and $u(x)$ is the dimensionless flow velocity profile. Eqn. 2 can be solved in a general form for $-1 \leqslant x \leqslant 1$, $z \geqslant 0$, $C(x, 0) = C_0(x_0)$, provided that at the channel walls, *i.e.*, at $x = \pm 1$, the driving force $\varphi(x)$ is directed inside the channel. Using a standard approach [20], we obtain the following equations of characteristics for eqn. 2:

$$\frac{dx}{ds} = \varphi(x); \qquad \frac{dz}{ds} = \mu u(x); \qquad \frac{dC}{ds} = -C \cdot \frac{d\varphi(x)}{dx} \tag{3}$$

where s is a variable parameter. Solving eqns. 3, we obtain

$$z = \mu \int_{x_0}^{x} \frac{u(x)}{\varphi(x)} dx; \qquad z_0 = 0 \tag{4}$$

$$C(x, z) = C_0\{x_0(x, z)\} \frac{\varphi\{x_0(x, z)\}}{\varphi(x)}$$

As can be seen from comparison with eqn. 2, the first of eqns. 4 is actually the particle trajectory equation. It relates the transient (at a given z) lateral coordinate x of a particle to its starting coordinate x_0 (at $z = 0$) and *vice versa:* $x = x(x_0, z)$, $x_0 = x_0(x, z)$.

Eqns. 4 describe the stationary (but non-equilibrium in essence) concentration distribution of particles over the channel flow in the kinematic (non-diffusive) approximation for an arbitrary velocity profile of laminar flow in a flat channel and arbitrary lateral profile of a transverse force homogeneous along the channel. These equations show that the shape and other characteristic features, such as positions of maxima of the transient lateral concentration profiles, depend strongly on the force and velocity profiles, $\varphi(x)$ and $u(x)$, distance along the channel z and particle characteristic μ. This situation differs from the laterally equilibrium one, where the concentration maxima have a Gaussian shape and their positions do not depend on z [9–14].

We shall analyse the shape of non-equilibrium concentration profiles, determined by eqns. 4, for the simplest and most relevant for our experiments symmetrical case, when $u(x) = u(-x)$ and $\varphi(x) = -\varphi(x)$. In this case only the $0 \leqslant x \leqslant 1$ interval needs to be considered. We shall assume also that the transverse force focuses the particles at some plane $x = x_f$ (and, of course, at the symmetrical plane $x = -x_f$) which are parallel to the channel walls:

$$\varphi(x) = \begin{cases} -|\varphi(x)|, & x_f < x \leqslant 1 \\ |\varphi(x)|, & 0 < x \leqslant x_f \end{cases} \tag{5}$$

For such force profiles, as can be seen from eqns. 4, the following inequalities are valid for all $z > 0$: if a starting coordinate $x_0 < x_f$, then $x(x_0, z) > x_0$, but if $x_0 > x_f$, then

$x(x_0, z) < x_0$. The latter means the existence of a boundary trajectory $x = x_m(z)$ such that $C(x, z) \equiv 0$ for $x > x_m(z)$. This trajectory starts from $x_0 = 1$ and is described by

$$z = \mu \int_1^{x_m} \frac{u(x)}{\varphi(x)} dx \equiv \mu \Phi(x_m) \tag{6}$$

The curve of eqn. 6 defines the position of the peripheral sharp edge of the transverse concentrational distribution of particles in a flow. Owing to the action of the transverse force, this distribution detaches from the channel walls and changes its initial shape in the course of advancement of particles along the channel. The fraction characteristic parameter μ does not enter the $\Phi(x_m)$ in eqn. 6, so the relationship $z = \Phi(x_m)$ is the universal (apparatus) function: the edge position of the concentration profile for any fraction can be obtained from this function after multiplication by μ.

Using eqns. 4–6, it is possible to draw some general conclusions about the shape of $C(x, z)$. We shall start with the concentration values at the channel axis and at the peripheral edge of the concentrational distribution. As follows from eqns. 4, for $x(x_0, z) \to 0$ with $z =$ constant, the starting coordinate $x_0(x, z)$ also tends to zero. Setting $x \to 0$ and $x = x_m$ in eqns. 4, we obtain correspondingly:

$$\begin{aligned} C(0, z) &= C_0(0) \lim_{x \to 0} \frac{\varphi\{x_0(x, z)\}}{\varphi(x)} \\ C(x_m, z) &= C_0(1) \frac{\varphi(1)}{\varphi(x_m)} \end{aligned} \tag{7}$$

Thus, depending on the specific form of the force profile (eqn. 5), concentration profiles both falling and rising to the channel walls are possible. Accordingly, the edge singularity of $C(x, z)$ at $x = x_m(z)$ may be of peak or step type. This can be solved proceeding from the sign of the derivative $\partial C(x, z)/\partial x$ with $z =$ constant. Let $C_0(x_0)$ be constant at the channel entrance. Taking the derivative of eqns. 4, we obtain

$$\frac{\partial C(x, z)}{\partial x} = C_0 \frac{\varphi(x_0)\varphi'_x(x_0)}{[\varphi(x)]^2} \left[\frac{u(x)}{u(x_0)} - \frac{\varphi'_x(x)}{\varphi'_x(x_0)} \right] \tag{8}$$

where x and x_0 are related by eqns. 4. The distribution edge lies at $x > x_f$, where $x(x_0, z) < x_0$ for all $z > 0$. For a plane-symmetrical flow that means that $u(x) > u(x_0)$. Hence the sign of eqn. 8 depends completely on the signs of the first and second derivatives of the force profile, φ'_x and φ''_x. For example, if $\varphi'_x = 0$ [$\varphi(x) =$ constant], then $\partial C(x, z)/\partial x = 0$ and the concentration profile keeps a rectangular shape, shrinking to the focusing planes with increase in z. In the case when $\varphi'_x < 0$ and $\varphi''_x < 0$, which corresponds to the force rapidly falling inside the channel, $\partial C(x, z)/\partial x > 0$, so the concentration profile has the peak at $x = x_m(z)$.

Together with the shapes of transient concentrational profiles, another important factor in dealing with the non-equilibrium situation is the effective distance z_f from the channel entrance corresponding to the establishment of lateral equilibrium in

the particles' system in a flow. This characteristic, in addition to the shape and height of the peripheral edge singularity of $C(x, z)$ in the limit of lateral equilibrium, is defined by behaviour of $\varphi(x)$ near the focusing point. Taking into account that at this point $\varphi(x) = 0$, we can write in general form, for $(x - x_f) \ll 1$,

$$\varphi(x) \approx -\varphi_0(x - x_f)^\alpha, \qquad \varphi_0 > 0, \alpha > 0 \tag{9}$$

The value of the equilibrium distance z_f can be defined formally by the integral in eqns. 4, taken from 1 to x_f. For $\alpha < 1$ in eqn. 9 this integral is finite, but for $\alpha \geqslant 1$ it diverges. Formally this means that full equilibrium sets at $z \to \infty$. In reality, the registered singularities of $C(x, z)$ (peak or step) have a finite width Δ (in units of h) which is determined by diffusive and instrumental broadening. Hence in practice it is sufficient to use an effective value of z_f corresponding to $x_f + \Delta$ as the upper limit of integration in eqns. 4. If $\Delta \ll 1$, then an approximate expression for z_f can be obtained, in addition to asymptotic relationships for $x_m(z)$ and $C(x, z)$, valid for large $z \approx z_f$. Integrating in eqns. 4 and taking into account that the nearest vicinity of x_f gives the main contribution to the result, we obtain approximately:

for $\alpha = 1$:

$$z_f \approx \frac{\mu u(x_f)}{\varphi_0'} \ln\left(\frac{1}{\Delta}\right); \qquad x_m(z) \approx x_f + \exp\left(-\frac{\varphi_0 z}{\mu u(x_f)}\right);$$

$$C(x_m, z) \approx C_0(1)\frac{|\varphi(1)|}{\varphi_0}\exp\left[\frac{\varphi_0 z}{\mu u(x_f)}\right] \tag{10}$$

for $\alpha > 1$:

$$z_f \approx \frac{\mu u(x_f)}{(\alpha - 1)\varphi_0}\left(\frac{1}{\Delta}\right)^{\alpha - 1}; \qquad x_m(z) \approx x_f + \left[\frac{\mu u(x_f)}{(\alpha - 1)\varphi_0 z}\right]^{\frac{1}{\alpha - 1}};$$

$$C(x_m, z) \approx C_0(1)\frac{|\varphi(1)|}{\varphi_0}\left[\frac{(\alpha - 1)\varphi_0 z}{\mu u(x_f)}\right]^{\frac{\alpha}{\alpha - 1}}$$

Eqns. 10 show, that for large particles ($\Delta \gg 1$) and weak lateral fields ($\mu \gg 1$), the equilibration distance can be very long. For smaller distances $z < z_f$, the height $C(x_m, z)$ of a concentration peak increases and its width decreases with increase in z, while the peak position $x_m(z)$ approaches the focusing point x_f, obeying simular laws. Thus, eqns. 10 describe in a non-diffusive approximation the final stage of transverse equilibration in a particle system in a flow and the transition to the stationary lateral concentration profiles usually considered as a starting point in FFFF theory [8–14]. For traditional FFFF systems with primary and secondary fields, and also for the system with an intrinsic hydrodynamic force, the power index α in eqns. 9 and 10 is equal to unity.

We shall now consider the resolving power of FFFF with IDA detection for

a laterally non-equilibrium situation; the equilibrium situation was considered previously [2]. The distance between the peaks of two fractions in the IDA spectrum is determined by the difference in flow velocities at the lateral positions of their concentration peaks [2]. These positions are $x_m(z, \mu)$, described by eqn. 6 for appropriate μ. Let two fractions in a flow have characteristic parameters μ and $(\mu + \delta\mu)$. Then the distance between the corresponding Doppler peaks [2,3] is

$$\Delta\omega_D = q[v_z(x_2) - v_z(x_1)] \approx q v_{\parallel} u'_x(x_m) \frac{\partial x_m}{\partial \mu} \delta\mu \tag{11}$$

Here $q = (4\pi n_0/\lambda_0)\sin(\vartheta/2)$ is the scattering wavenumber, n_0 the refractive index of the carrier fluid, λ_0 the vacuum wavelength of the probing laser light and ϑ the scattering angle [3].

The spectral width of Doppler lines in the non-diffusive case being considered is determined by the finite time of particle transit through the probing laser beam. For a Gaussian beam with characteristic width b, this instrumental broadening is $\Delta_i = (v_{\parallel}/b)u(x_m)\cos(\vartheta/2)$. Adopting as the resolution criterion of the two adjacent peaks the condition $\Delta\omega_D = 2\Delta_i$ and using eqn. 6 for derivation of $\partial x_m/\partial\mu$, we obtain

$$\frac{\partial\mu}{\mu} = \frac{\lambda_0}{2\pi n_0 b \tan(\vartheta/2)} \left| \frac{u(x_m)\Phi'_x(x_m)}{u'_x(x_m)\Phi(x_m)} \right| \tag{12}$$

Eqn. 12 defines the relative or differential resolving power of the method. It depends on the IDA measuring geometry, the particle parameter μ and specific forms of the force and velocity profiles. As follows from eqn. 12, it is preferable to do the measurements at large scattering angles, with broad laser beams and small light wavelengths. It can also be seen that, owing to the z-dependence of eqn. 12, the best resolution for a given μ is obtained at some optimum distance z_0 from the channel entrance, where eqn. 12 reaches its minimum. The value of z_0 turns out to be strongly dependent on the particle parameter μ. Considering the analysis of mixtures with a broad fraction distribution over μ, this means the possibility of optimization of resolving conditions for some preselected intervals of μ values by variation of the distance z_0.

Intrinsic hydrodynamic force in Poiseuille flow

We now apply the general relationships obtained above to the focusing FFF version, based on the use of an intrinsic hydrodynamic force acting on the particles in Poiseuille flow. Substituting into eqns. 4 eqn. 1 for the profile of this force, and $u(x) = 1 - x^2$ for the flow velocity profile, we obtain the following expressions for the particle trajectories and concentration distribution over the channel:

$$z^*\left(\frac{a}{h}\right)^3 = \frac{1 - x_f^2}{x_f^2}\left[\ln\left(\frac{x}{x_0}\right) + \frac{1 - x_f^2}{2}\ln\left(\frac{x_f^2 - x_0^2}{x_f^2 - x^2}\right)\right];$$

$$C(x, z^*, a) = C_0(x_0)\frac{x_0(x_f^2 - x_0^2)}{x(x_f^2 - x^2)}; \qquad z^* = \frac{3 v_{\parallel} \rho_0 h}{8\eta} z; \tag{13}$$

$$C(x, 0) = C_0(x_0), \quad -1 \leqslant x, x_0 \leqslant 1, \quad z^* \geqslant 0$$

Here the new dimensionless coordinate z^* is introduced to make more convenient the comparison of the trajectories of particles of different size a. The boundary trajectory $x_m(z^*, a)$ (eqn. 6) which determines the concentration peak position corresponds to $x_0 = 1$ in eqn. 13. As follows from substitution of eqn. 1 into eqn. 8, the transient transverse concentration profile is strongly asymmetric, rising continuously from the centre to the channel walls and having sharp cut-offs at $|x| = x_m(z^*, a)$.

Fig. 1 shows the variations of the position and height of concentration peaks with the distance along the channel, computed according to eqn. 13 for particles of various relative size (a/h). Actually, these curves illustrate the process of transverse equilibration of various particle fractions in a flow under the action of an intrinsic hydrodynamic force. One can see that at large distances $z^* \gg 10^3$, *i.e.*, in the equilibrium state, all the peaks merge together, but at intermediate distances they are well separated across the channel. This is due to the fact that the focusing force depends strongly on the particle size: $F_0 \approx (a/h)^4 v_\parallel^2$ (eqn. 1). The equilibration distance along the channel and other features of the limiting behavior of $C(x, z^*, a)$ are determined by eqns. 9 and 10 with $\varphi_0 = 2x_f^2$, $\alpha = 1$ and

$$\mu = \frac{8\eta(1 - x_f^2)}{3v_\parallel \rho_0 h}\left(\frac{a}{h}\right)^{-3} \tag{14}$$

Fig. 1b shows such a limiting exponential behaviour of $C(x_m)$. From eqn. 10 the fraction's equilibration distance is given by

$$z_f = \frac{4\eta(1 - x_f^2)^2}{3v_\parallel \rho_0 x_f^2 h}\left(\frac{a}{h}\right)^{-3} \ln\left(\frac{1 - x_f^2}{2x_f \Delta}\right) \tag{15}$$

For particle size $a > 1$ μm the diffusive broadening can be neglected compared with the IDA instrumental broadening, which gives $\Delta = [\lambda_0/n_0 b \tan(\vartheta/2)](1 - x_f^2)/4x_f$ (see eqn. 12). Thus, eqn. 15 shows that for $\lambda_0 = 0.63$ μm, $b \approx 10^{-2}$ cm, $\vartheta \approx 0.2$ rad and for

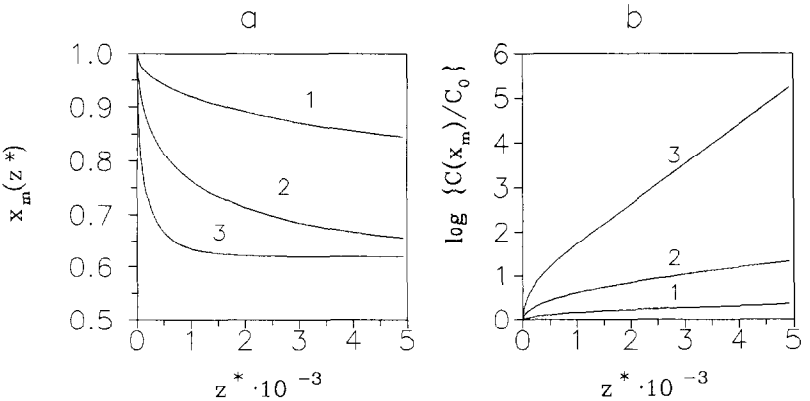

Fig. 1. (a) Calculated transverse position, $x_m(z^*)$, and (b) relative height, $C(x_m)/C_0$, of the peak of transverse concentration of particles, placed in a plane Poiseuille flow in a narrow channel. Relative size (a/h): (1) 0.01; (2) 0.05; (3) 0.1.

(typical in our experiments) flow velocities $v_{\|} \approx 1$ cm/s, channel widths $h \approx 10^{-2}$ cm and particle relative sizes $a/h \approx 10^{-2}$–10^{-1}, the transverse equilibration of particles due to the action of intrinsic hydrodynamic force completes at distances $z_f h > 10^4 h \approx 10^2$ cm from the channel entrance. On the other hand, Fig. 1 shows that efficient separation of fractions takes place at distances $z^* \approx 500$, *i.e.*, $zh \approx 5$ cm. One can see also that for each pair of the discrete set of fractions there exists a specific distance z_0^* which ensures the optimum spatial separation of these two fractions.

Let us now consider further the polydisperse system of particles with a discrete set of fractions and make a natural assumption that these fractions have the normal size distribution near the appropriate mean values. It is sufficient to consider a binary mixture, because the generalization is obvious. In this instance the stationary concentration of particles $C_0(x_0)$ maintained at the channel entrance has the form

$$C_0(a) = \frac{1}{\sqrt{2\pi}}\left\{\frac{n_1}{\sigma_1}\exp\left[-\frac{(a-a_1)^2}{2\sigma_1}\right] + \frac{n_2}{\sigma_2}\exp\left[-\frac{(a-a_2)^2}{2\sigma_2}\right]\right\} \tag{16}$$

where n_i is a relative concentration, a_i is a mean fraction size and σ_i is a distribution width, $i = 1, 2$. {Do not confuse eqn. 16 with a Gaussian-type stationary lateral concentration distribution, usually considered in FFFF [9,11], because $C_0(x_0)$, set by eqn. 16, is homogeneous across the channel!} Then the transient concentration profile of the polydisperse (binary) mixture C_{pd} at some distance z^* (say, at the optimum separation distance z_0^*) can be obtained by integrating over a the elementary profile $C(x, z^*, a)$, set by eqn. 13:

$$C_{pd}(x, z_0^*) = \int_0^\infty C_0(a)\, C(x, z_0^*, a)\, \mathrm{d}a \tag{17}$$

Fig. 2 presents the total and fractional concentration profiles, computed for various relative concentrations of fractions, using eqns. 13, 16 and 17. It can be seen that the fractional profiles are strongly asymmetric relative to their peak positions, which is due to the absence of equilibrium across the channel.

Fig. 3 shows the corresponding IDA spectra, which would be registered at point z_0^* of a channel for the particle transverse concentration profiles presented in Fig. 2. These spectra are computed as follows. For the monodisperse system of scatterers with a negligibly small diffusive motion, the shape of the IDA spectrum is related to the concentration profile of scatterers in a flow by the following equation [1–3]:

$$S(\omega, z^*, a) \sim a^3 \Psi(qa) \int_{-1}^{1} C(x, z^*, a)\delta[\omega - q v_{\|} u(x)]\mathrm{d}x \tag{18}$$

where the factor $a^3\Psi(qa)$ is responsible for the scattering angle and particle volume dependence of the scattered light intensity. To obtain the IDA spectrum for a polydisperse system with a size distribution described by $C_0(a)$ (eqn. 16), eqn. 18 should be integrated over a with $C_0(a)$ as a weight function. In the case of Poiseuille flow, when $u(x) = 1 - x^2$, this gives

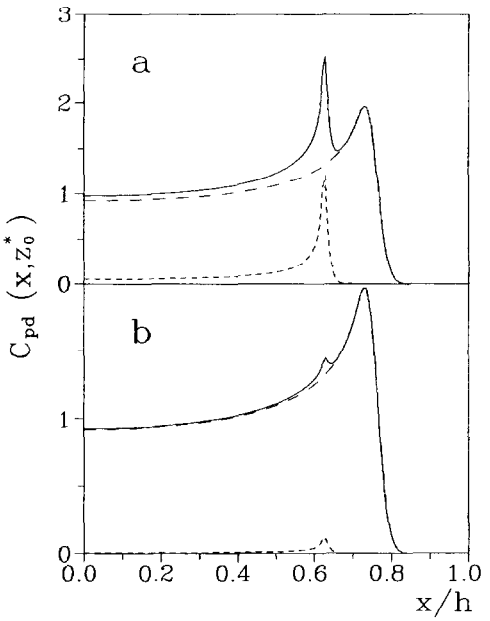

Fig. 2. Transverse concentration profiles (solid line, total; dashed lines, fractional) at the optimum distance of intrinsic hydrodynamic FFFF, computed for a binary mixture of particles with $a_1 = 0.05h$, $\sigma_1 = 0.1a_1$, $a_2 = 0.1h$, $\sigma_2 = 0.1a_2$ (see text). Relative fraction concentrations: (a) $n_1/n_2 = 10$; (b) $n_1/n_2 = 100$.

$$S_{pd}(\omega, z^*) \sim \frac{1}{\omega_0\sqrt{1-\dfrac{\omega}{\omega_0}}} \int_0^\infty a^3 \Psi(qa)\, C_0(a)\, C\left(\sqrt{1-\frac{\omega}{\omega_0}}, z^*, a\right) da \tag{19}$$

$$\omega_0 = q v_{\parallel}, \quad 0 \leqslant \omega \leqslant \omega_0$$

As eqns. 18 and 19 show, the presence of a δ-function in eqn. 18 leads to the substitution $x = \sqrt{1 - \omega/\omega_0}$ in the concentration profile $C(x, z^*, a)$ after the integration over x. This gives the formal relationship between this profile and the shape of the IDA spectrum. Physically it reflects the fact that the contribution to the integral spectrum from each point of the scattering volume of a flow is the Doppler line whose frequency is determined by the local flow velocity, while the intensity is proportional to the local concentration of scatterers. Eqns. 18 and 19 are written in the simplest way, which does not account for the diffusive and instrumental broadening. For the computation of IDA spectra presented in Fig. 3, more sophisticated equations were used, which take into account the instrumental broadening due to the finite time of particle transit through the scattering volume (the part of a channel illuminated by a probing laser beam).

As can be seen from Figs. 2 and 3, in the case of a homogeneous particle distribution the spectrum has a shape that is characteristic of the one-dimensional Poiseuille velocity profile and is determined by the $(1 - \omega/\omega_0)^{-1/2}$ factor in eqn. 19.

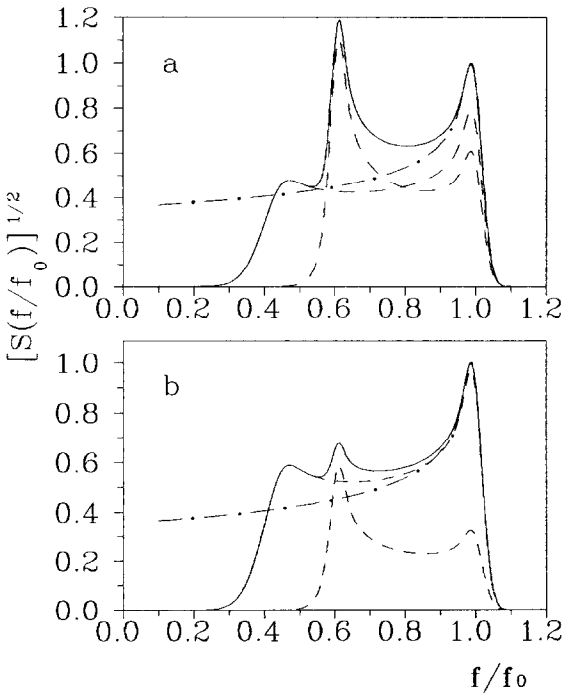

Fig. 3. Integral Doppler spectra of the binary suspension flow in a flat channel, computed for the particle concentration profiles of Fig. 2 (solid and dashed lines) and for a homogeneous particle distribution (dot-dashed line).

However in the case when the transverse particle concentration in a flow has maxima, the integral Doppler spectrum possesses the corresponding peaks. From comparison with Fig. 2 it is seen that IDA recording greatly enhances the peaks corresponding to the larger particles. This is due to the a^3 factor in the light-scattering intensity (eqns. 18 and 19).

EXPERIMENTAL

The measurements were carried out using a demountable flat channel 75 mm long and 8 mm high, formed by two polished glass plates separated by spacers. The channel width $2h$ was set by spacers and varied from 40 to 120 μm in different experiments. The channel was included in a closed circuit between the upper and the lower reservoirs, which were connected by a peristaltic pump. The measured samples were dilute suspensions (10^5–10^7 particles/cm^3) of latex particles 4 μm diameter, human erythrocytes and their mixtures in a standard phosphate-buffered saline (pH 7.3–7.5). The flow velocity, controlled by the height of the upper reservoir, was $5 \div 8$ cm/s at the channel axis. The IDA spectra of a laminar suspension flow were recorded using the differential optical set-up and the installation described elsewhere [3,4]. The spectra, registered in the two-beam optical set-up, contain the Doppler lines which can be detected in the two-beam (heterodyne) mode of operation only, and the intense line

centred at zero frequency, which is present in the single-beam mode also. This line originates from the time variations of the particle illumination during its transit through the focused laser beam. Therefore, to obtain the IDA spectrum proper, sequential recording of the two-beam and single-beam spectra were carried out each time, with subsequent subtraction of the second from the first in a proper scale. The spectra recorded were the amplitude Doppler spectra $[S(f)]^{1/2}$ ($f = \omega/2\pi$ = frequency in Hz) recorded in the accumulation mode with averaging of *ca.* 10^4 subsequent samplings. The point of recording was 65 mm away from the channel entrance.

Fig. 4 shows the IDA spectra thus obtained for two-component suspension flow for various relative concentrations of the components (latex particles and erythrocytes). As can be seen from comparison with Figs. 2 and 3, in all instances transverse focusing of particles by the intrinsic hydrodynamic force is taking place, each fraction being represented by its own peak in the spectrum. The characteristic size of an erythrocyte particle is 7–8 μm, depending on its physiological condition, whereas the latex particle size is 4 μm. Hence the action of the transverse force (eqn. 1) is about one order of magnitude stronger with erythrocytes, resulting in considerably faster focusing of their fraction. The situation is closely simulated by curves 2 and 3 in Fig. 1. As a result, the erythrocyte peak appearing in the IDA spectrum as erythrocytes are added to the latex suspension is situated at a higher frequency than the latex peak. With increase in erythrocyte concentration the peak rapidly grows and begins to

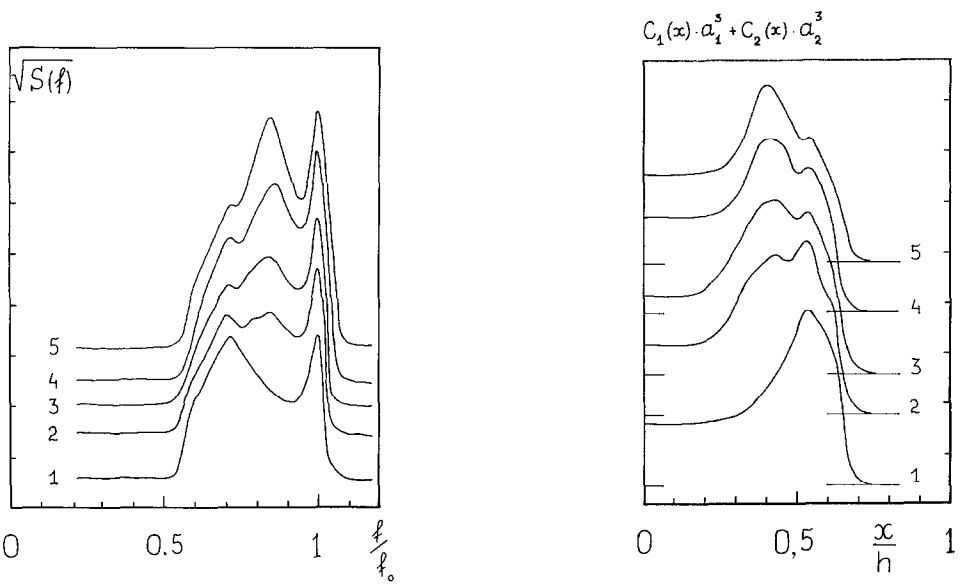

Fig. 4. IDA spectra of a dilute suspension flow of latex particles ($2a$ = 4 μm) and human erythrocytes ($2a \approx 7$ μm) in a flat channel ($2h$ = 47 μm), measured for various relative concentrations of latex (n_1) and erythrocytes (n_2): n_2/n_1 (1) = 0; (2) 0.05; (3) 0.1; (4) 0.15; (5) 0.2.

Fig. 5. Transverse profiles of the sum of the local fraction volumes, $C_1(x)a_1^3 + C_2(x)a_2^3$ (relative units), evaluated for mixtures of latex particles and erythrocytes in a flow, using the IDA spectra in Fig. 4.

dominate in the spectrum. This is a consequence of the cubic law of the scattered light intensity *versus* particle size dependence (see eqns. 18 and 19).

Using the relationships of the type of eqns. 18 and 19 between the IDA spectrum shape and the light scattering particles concentration profile, it is possible to evaluate such profiles for the latex particles and erythrocytes in measured suspension flows on the basis of the spectra in Fig. 4. The corresponding results are presented in Fig. 5. They are in good agreement with the theoretical calculations (Fig. 2), except for the peak positions, which is due to the value $x_f = 0.62$, used in calculations. As was pointed out (see eqn. 1), under our experimental conditions the focusing point lies closer to the channel centre than was measured [18] and calculated [19]. This phenomenon is now under investigation.

Hence the results of the present measurements show that under the experimental conditions the lateral spatial separation of a binary mixture (latex particles–erythrocytes) into two nearly monodisperse fractions occurs as a result of the action of the intrinsic focusing hydrodynamic force in a channel flow.

DISCUSSION AND CONCLUSIONS

The theoretical analysis and experimental data presented here have two main aspects. First, they introduce a new focusing force into FFFF practice [8–17], namely, the intrinsic hydrodynamic (or Segre–Silberberg) force [18,19], which allows analytical fractionation of particles relative to their size to be accomplished without the application of any external field to a channel. Second, they demonstrate the practical possibility of analytical fractionation of particles not only after their equilibration across the channel, but also in the process of this equilibration. Such a possibility is now opened up owing to the application of the IDA recording technique [1–4] just inside the channel. The application of IDA also allows the analysis time to be decreased to *ca.* 1 min.

The new experimental conditions require an adequate description of the process of particle equilibration across the channel, which usually assumed to be completed before the separation starts along the channel [5–17]. The process of transverse equilibration was considered in this paper, using the kinematic or non-diffusive approximation. Such an approach is well justified when dealing with sufficiently large (micrometre-sized) particles, and has the serious advantage of giving easy-to-interpret analytical results for the general form of lateral force and flow velocity profiles in a channel. The next step, which is under development, is to consider the appropriate convective diffusion equation, but this requires numerical procedures. The present results in their limiting case, *i.e.*, for large distances along the channel, are consistent with the initial steady-state concentrational distributions, considered by Giddings [9] and Janča and Chmelik [11], if the latter are characterized by negligibly small diffusion.

The present separation experiments using the intrinsic hydrodynamic force were carried out under essentially non-equilibrium lateral conditions, but they can be done in the usual FFFF mode of operation, when the fractions are detected at the outlet of a channel after their lateral equilibration and longitudinal separation. The theoretical estimates and preliminary experiments showed, however, that in the equilibrium mode of operation the longitudinal separation of particles is very difficult to observe, primarily because the equilibrium focusing positions are identical for all the particles

regardless their size [18,19]. In contrast, as the present theoretical and experimental data show (see eqns. 1 and 13 and Figs. 1–5), in the non-equilibrium mode it is possible to obtain the effective transverse separation of micrometre-sized particles using channel widths of several tens of micrometres and channel lengths of several centimetres. By increasing the length and decreasing the width of a channel, it seems to be possible to accomplish the non-equilibrium intrinsic hydrodynamic FFFF of submicrometre-sized particles also.

The use of the intrinsic hydrodynamic force together with IDA recording in FFFF gives another promising possibility, namely the detection of low concentrations of large-sized particles in a mixture. The possibility of such indicative FFFF is based on the fact that the magnitude of the focusing hydrodynamic force (eqn. 1) is proportional to the fourth power of particle size, and the scattered light intensity, registered from the particle in IDA, is proportional to the cube of its size. These two factors result in the situation that the peak in the IDA spectrum corresponding to admixture of larger particles in a flow can be observed distinctly, almost independently of the specific form of the size distribution function of smaller particles.

Owing to the focusing character of the intrinsic hydrodynamic force, the most advantageous applications of intrinsic hydrodynamic FFFF are to mixtures with discrete sets of fractions. In this instance, as eqns. 16–19 show, the recording of IDA spectra allows not only the identification of different fractions, but also the comparatively easy determination of their concentration profiles in a flow and their relative concentrations from the shape of the IDA spectra. However, in the case of continuous particle size distribution functions, the solution of such inverse problem becomes complicated and requires the application of the theory of inverse incorrect mathematical problems. A similar situation arises in dynamic light scattering when applied to the analysis of polydisperse particle systems [21].

SYMBOLS

a	radius of a particle
b	Gaussian width of a laser beam
$C(x, z)$, $C(x, z^*, a)$	concentration of particle fraction in a flow
$C(x_0)$	stationary concentration at the channel entrance
$C_{pd}(x, z)$	concentration of polydisperse particle mixture
F_x, F_0	lateral force and its magnitude
f	frequency in Hz
h	half-width of a flat channel
n_0	refraction index of fluid
n_1, n_2	relative concentrations of fractions in a binary mixture
q	laser light-scattering wavenumber
$S(\omega, z^*, a)$, $S_{pd}(\omega, z^*)$	IDA power spectra at a distance z^*
$u(x)$	velocity profile of a channel flow
$\vec{v}$	particle velocity relative to the channel walls
$v_{\|\|}$	maximum flow velocity
x	lateral coordinate of a particle (in units of h)
x_f	focusing point position
z	particle coordinate along the flow (in units of h)

z^*	reduced-to-flow-parameters z coordinate
z_f	effective distance, corresponding to lateral equilibration
z_0^*	distance corresponding to optimum lateral separation
α	power index of lateral force's serial expansion near x_f
Δ	concentration peak effective width (in units of h)
η	fluid viscosity
ϑ	laser light-scattering angle
λ_0	wavelength of laser light
μ	separation parameter of a particle
ρ_0	fluid density
σ	effective width of particle size distribution function
$\Phi(x_m)$	peak position universal function
$\Psi(qa)$	light-scattering indicatrix
$\omega = 2\pi f$	cyclic frequency; $\omega_0 = qv_{\|\|} = 2\pi f_0$

REFERENCES

1 V. L. Kononenko and S. N. Semyonov, *Zh. Fiz. Khim.*, 60 (1986) 2553.
2 S. N. Semyonov and V. L. Kononenko, *Zh. Fiz. Khim.*, 61 (1987) 1947.
3 S. N. Semyonov, V. L. Kononenko and Ya. K. Shimkus, *J. Chromatogr.*, 446 (1988) 141.
4 V. L. Kononenko and Ya. K. Shimkus, *Pis'ma Zh. Tekh. Fiz.*, 14 (1988) 2064.
5 J. C. Giddings, *Sep. Sci.*, 1 (1966) 123.
6 J. C. Giddings, *Sep. Sci.*, 19 (1984–85) 831.
7 J. Janča, in Z. Deyl (Editor), *Separation Methods*, Elsevier, Amsterdam, 1984, p. 497.
8 J. Janča, *Makromol. Chem., Rapid Commun.*, 3 (1982) 887.
9 J. C. Giddings, *Sep. Sci.*, 18 (1983) 765.
10 J. Janča and V. Jahnova, *J. Liq. Chromatogr.*, 6 (1983) 1559.
11 J. Janča and J. Chmelik, *Anal. Chem.*, 56 (1984) 2481.
12 J. C. Giddings, *Sep. Sci.*, 21 (1986) 831.
13 M. R. Schure, K. D. Caldwell and J. C. Giddings, *Anal. Chem.*, 58 (1986) 1509.
14 S. N. Semyonov, A. A. Kuznetsov and P. P. Zolotaryov, *J. Chromatogr.*, 364 (1986).
15 J. Chmelik and J. Janča, *J. Liq. Chromatogr.*, 9 (1986) 55.
16 J. Janča and N. Novakova, *J. Liq. Chromatogr.*, 10 (1987) 2869.
17 J. Janča and N. Novakova, *J. Chromatogr.*, 452 (1988) 549.
18 G. Segre and A. Silberberg, *J. Fluid Mech.*, 14 (1962) 15.
19 P. Vasseur and R. G. Cox, *J. Fluid Mech.*, 78 (1976) 385.
20 G. A. Korn and T. M. Korn, *Mathematical Handbook for Scientists and Engineers*, McGraw-Hill, New York, 1961.
21 B. Chu and A. Dinapoli, in B. E. Dahneke (Editor), *Measurements of Suspended Particles by Quasielastic Light Scattering*, Wiley, New York, 1983, p. 81.